Orthorhombic distortion of Rb_2MnCl_4 in its antiferromagnetic phase

1992 J. Phys.: Condens. Matter 4 2281

(http://iopscience.iop.org/0953-8984/4/9/022)

J. Phys.: Condens. Matter 4 (1992) 2281–2295. Printed in the UK

Orthorhombic distortion of Rb_2MnCl_4 in its antiferromagnetic phase

H Greb†, T Pabst†, M Rothaler†, A A Mukhin‡, A Yu Pronin‡, K Strobel§ and R Geick†

† Physikalisches Institut, Universität Würzburg, Am Hubland, 8700 Würzburg, Federal Republic of Germany

‡ General Physics Institute, Academy of Sciences of the USSR, Vavilov Street 38, 117942 Moscow, USSR

§ MBB Apparate, 8012 Ottobrunn, Federal Republic of Germany

Received 30 October 1991

Abstract. Rb_2MnCl_4 was always considered to be an ordinary quasi-two-dimensional uniaxial weakly anisotropic antiferromagnet with the crystallographic c axis as the easy axis. This picture became dubious when a splitting was observed of one of the magnetic modes for an external magnetic field applied perpendicular to the c axis. New magnetic resonance measurements revealed also a splitting of the zero-field antiferromagnetic resonance. All the unexpected phenomena observed in our investigation can be explained in terms of an orthorhombic distortion of Rb_2MnCl_4 in its antiferromagnetic state, taking into account that all samples are of the multi-domain type below the Néel temperature.

1. Introduction

Perovskite-type layer structures like Rb_2MnCl_4 and K_2MnF_4 are quasi-two-dimensional antiferromagnets [1–3] with the K_2NiF_4 crystal structure $I4/mmm$ (D_{4h}^{17}). In the antiferromagnetic long-range three-dimensional order below the Néel temperature (T_N = 54.8 K for Rb_2MnCl_4), the symmetry in these materials is reduced from tetragonal to orthorhombic. There are two antiferromagnetic domains with the structures $Acam + Acam \times (\Theta|\tau)$ and $Bbcm + Bbcm \times (\Theta|\tau)$ [4], respectively, where Θ is the operation of time reversal and $\tau = (a/2, a/2, 0)$ is a non-primitive translation to be combined with this operation. The standard setting for the ordinary part of these space groups is $Cmca$ (D_{2h}^{18}). With respect to the tetragonal paramagnetic phase, the a and b axes are rotated by 45° in the orthorhombic structures, and the lattice constants are changed as $a_{new} = \sqrt{2}a_{old}$. The preferred spin direction or easy axis is the crystallographic c axis. The two domains (see figure 1) differ by the orientation of the spins in the $c/2$ plane. One domain is transformed to the other by reversing these spins, which has no influence on the antiferromagnetic order. A further difference between the two domains is that in the first ($Acam$) the ordered spins form ferromagnetic sheets perpendicular to the a axis and in the other domain ($Bbcm$), perpendicular to the b axis. The antiferromagnetic superreflections for the two domains are $(\frac{1}{2}, \frac{1}{2}, 0)$ and $(\frac{1}{2}, -\frac{1}{2}, 0)$, respectively. For spin-wave calculations and for the analysis of mangetic resonance data,

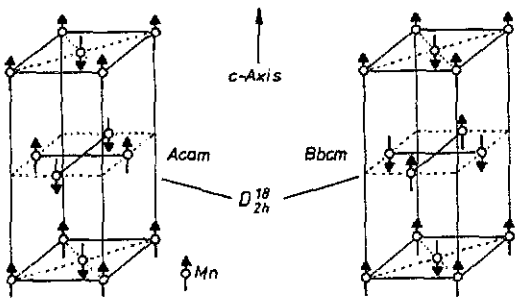

Figure 1. Antiferromagnetic structure of Rb_2MnCl_4 below $T_N = 54.8$ K; domain 1 (*Acam*) to the left and domain 2 (*Bbcm*) to the right. Only the Mn^{2+} ions are shown with their spin orientation.

it is usual to treat antiferromagnets like Rb_2MnCl_4 in the two-dimensional approximation because of their two-dimensional properties. For neutron scattering investigations however, it necessary to take the full three-dimensional structure and the two domains into account.

In the case of Mn^{2+} ions, the anisotropy energies are much smaller than the dominating intra-layer exchange interaction. Thus, Rb_2MnCl_4 can be considered a weakly anisotropic uniaxial antiferromagnet. The continuous spin-flop transition expected for these materials [5] has been confirmed experimentally also for Rb_2MnCl_4 [6]. The magnon dispersion relations of Rb_2MnCl_4 have been measured by inelastic neutron scattering [7]. The magnons at wavevector $q = 0$ have also been studied by magnetic resonance in the millimetre wave range [7, 8]. From the results of these investigations, it was concluded that Rb_2MnCl_4 is an ordinary uniaxial antiferromagnet with a doubly degenerate zero-field antiferromagnetic resonance (AFMR) mode and two linear Zeeman branches emerging from it for external magnetic fields parallel to the c-axis, one branch rising and the other falling [9]. At the spin-flop transition, these two branches pass into a field-dependent and a field-independent magnon mode in the spin-flop regime. The magnetic resonance studies have mostly been performed by sweeping the magnetic field at fixed frequency with an IMPATT oscillator as the millimetre wave source [10]. Two configurations have been available for these measurements, namely with the external magnetic field H_0 parallel to the crystallographic c axis ($H_0 \parallel c$) and with the external field perpendicular to it ($H_0 \perp c$).

While the experimental results for $H_0 \parallel c$ did not show any deviation from the results expected for a uniaxial easy-axis weakly anisotropic antiferromagnet, the experimental data for $H_0 \perp c$ were surprising and did not agree with the predictions from ordinary spin-wave calculations for such a system, namely one field-dependent mode rising in frequency with increasing field and one mode with a frequency independent of the magnetic field. Obviously, the latter cannot be observed in magnetic resonance by sweeping the magnetic field at fixed frequency. The unexpected feature in the experimental data for $H_0 \perp c$ is that we have observed a splitting of the field-dependent mode. Moreover, this splitting depends on the direction of the external magnetic field in the plane perpendicular to the c axis, described by the angle β between H_0 and the a-axis. Figure 2 shows this splitting as a function of β at a frequency of 129.4 GHz, not for Rb_2MnCl_4 but for the similar material $(CH_3NH_3)_2MnCl_4$, where Rb^+ has been replaced by $(CH_3NH_3)^+$ [11]. The same splitting was also observed in Rb_2MnCl_4, but at the higher frequencies necessary for Rb_2MnCl_4 not so complete with our IMPATT sources at that time. The oscillations in the magnetic field at resonance in figure 2 have been obtained by rotating the sample and thus varying the angle β between H_0 and the a axis. The

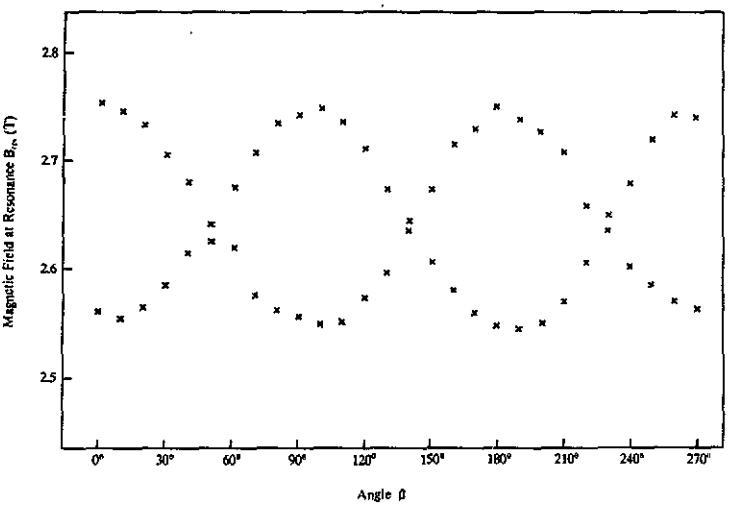

Figure 2. Antiferromagnetic resonance in $(CH_3NH_3)_2MnCl_4$. The magnetic field at resonance is shown for $\nu = 129.4$ GHz for the configuration $H_{ll} \perp c$ in dependence on the angle β between H_{ll} and the crystal a-axis.

observed splitting and the β dependence of the magnons cannot be understood on the basis of the usual theoretical considerations. The external magnetic field is much smaller than the internal exchange field, and it cannot force the spins considerably away from their preferred direction parallel to the c axis. Therefore, the field at resonance should not vary with β. Further, the one field-dependent magnon is not doubly degenerate and should therefore not split into two modes.

In order to gain some insight into these problems and eventually to solve them, we have started a thorough investigation of the magnetic excitations of Rb_2MnCl_4 by means of magnetic resonance. For this purpose, it was necessary to overcome the technical limitations of our equipment already mentioned. In addition to the IMPATT sources [10], we have been able to acquire backward-wave oscillators as sources for millimetre wave frequencies which are tunable over a wide range, nearly an octave. With these sources, it is possible to perform magnetic resonance also by sweeping the frequency at fixed or zero magnetic field or to choose the fixed frequency more appropriately when sweeping the magnetic field [12, 13]. A careful analysis of the experimental data obtained in this way, especially also a splitting of the zero-field AFMR, led us to the conclusion that there is an orthorhombic distortion in Rb_2MnCl_4 below the Néel temperature at which it is antiferromagnetically ordered. This orthorhombic distortion is believed to be due to magnetostrictive or magnetoelastic effects. The experimental data and the model considerations for the analysis and interpretation of these data are presented in this paper.

2. Experimental procedure

Our equipment for measuring magnetic resonance in the millimetre wave range has been described in detail elsewhere [10, 12, 13]. It consists of microwave and optical components as is typical for this spectral range. For most of the measurements discussed below, several backward-wave oscillators have been employed to cover the frequency

range 23–183 GHz. This millimetre wave range is most appropriate for magnetic resonance studies of the materials under consideration because the frequencies of the zero-field AFMR fall into this range. Magnetic fields up to 8 T are provided by a superconducting solenoid. With our instrumentation, we are able to study the magnetic resonance in various configurations [13]. For the layer-structured samples (Rb_2MnCl_4 etc.), the radiation always propagates parallel to the c axis of the crystal, i.e. perpendicular to the layers ($q \| c$). The possible configurations are then with the external magnetic field H_0 parallel to q and to the c axis (the Faraday configuration) or H_0 perpendicular to q and to the c axis (the Voigt configuration). The radiation incident to the sample is linearly polarized, and the direction of polarization can be rotated to excite the magnon to be measured in an optimum way. For magnetic resonance experiments, the direction of polarization of the magnetic field of the electromagnetic wave is very important.

Some of the experiments reported below have been performed with the sub-millimetre wave spectrometer 'Epsilon' in the General Physics Institute of the Academy of Sciences of the USSR in Moscow [14, 15]. Backward wave oscillators are also used as sources, and magnetic resonance has been observed by sweeping the frequency, unfortunately only at zero magnetic field.

The samples of Rb_2MnCl_4 single crystals were grown in quartz ampoules at the Universität Marburg by the Bridgeman method. Because of the sensitivity of these compounds to oxygen and moisture, all operations had to be performed under carefully purified inert gas (helium or argon). The quality of the single crystals was tested by x-ray and neutron diffraction.

3. Results for $H_0 \| c$

The unexpected splitting of the zero-field antiferromagnetic resonance of Rb_2MnCl_4 was first observed when the temperature dependence was studied with the submillimetre wave spectrometer 'Epsilon' in Moscow [14, 15]. The results (see figure 3) clearly show that there are two absorption lines which were found to be of magnetic origin as explained below. The transmission data $T(\nu)$ in figure 3 are the intensities transmitted by the sample without any normalization. Surprisingly, the two AFMR lines have unequal intensities. It is further puzzling that the transmission minima of these lines are lower than 50%. For a uniaxial antiferromagnet, however, the eigenvectors of the two magnetic modes near $H_0 = 0$ should exhibit right- and left-handed circular polarization. And for linearly polarized light incident to the sample, its transmission cannot drop below 50%. The $T(\nu)$ spectra in figure 3 have been analysed by means of a fit with a harmonic oscillator model [14] for the frequency dependence of the magnetic permeability in the range of the magnetic resonance

$$\mu(\nu) = 1 + \sum_k \Delta\mu_k \nu_k^2/(\nu_k^2 - \nu^2 + i\nu\Gamma_k) \tag{1}$$

where ν_k is the resonance frequency, Γ_k the damping constant determining the linewidth and $\Delta\mu_k$ the oscillator strength, i.e. the contribution to the static permeability, for the two modes with $k = 1$ and $k = 2$. The values of these parameters have been obtained from a fit to the experimental data. The fitting was performed under the assumption that the refractive index of Rb_2MnCl_4 is $n = 2.9$. It was found to be independent of polarization within experimental accuracy. The thickness of the sample was 0.98 mm. In figure 4, the temperature dependence is shown for the resonance frequencies ν_1 and

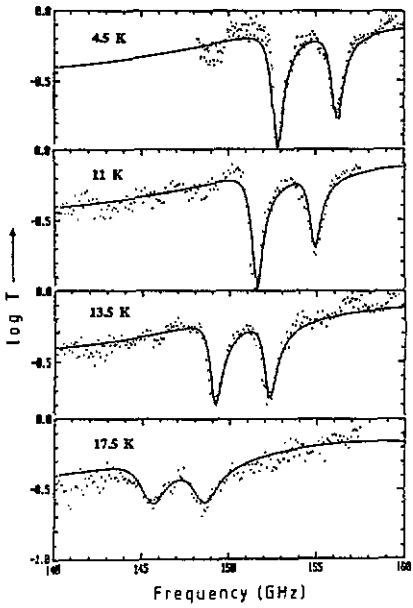

Figure 3. Zero-field splitting of the antiferromagnetic resonance in Rb_2MnCl_4: transmission curves (log T) versus frequency for various temperatures. These transmission data represent the intensities transmitted by the sample without any normalization.

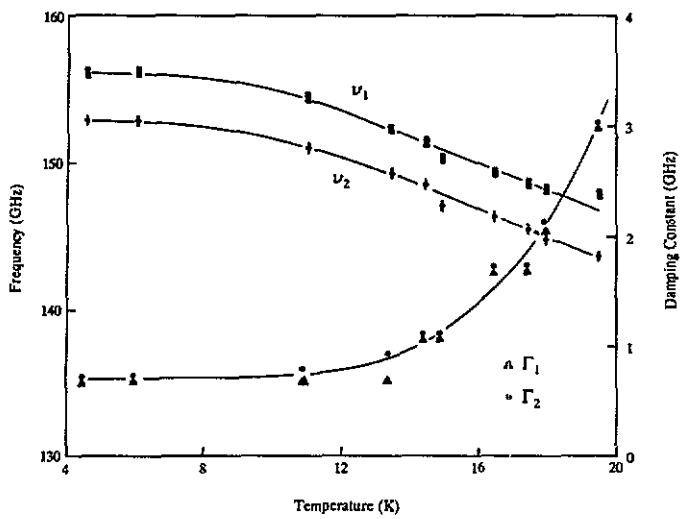

Figure 4. Harmonic oscillator fit to the experimental data in figure 3: resonance frequencies ν_1 and ν_2, damping constants Γ_1 and Γ_2 as a function of temperature.

ν_2 and for the damping constants Γ_1 and Γ_2. These temperature dependences show the typical behaviour of magnetic excitations, namely the frequencies decreasing and the linewidths increasing with increasing temperature towards the Néel temperature. The two oscillator strengths $\Delta\mu_k$ are practically independent of temperature, and their values are 0.6×10^{-3} and 0.8×10^{-3} respectively for the two modes.

Further studies were then performed with the millimetre wave spectrometer in Würzburg [12, 13] where the effects under consideration can be studied as a function of

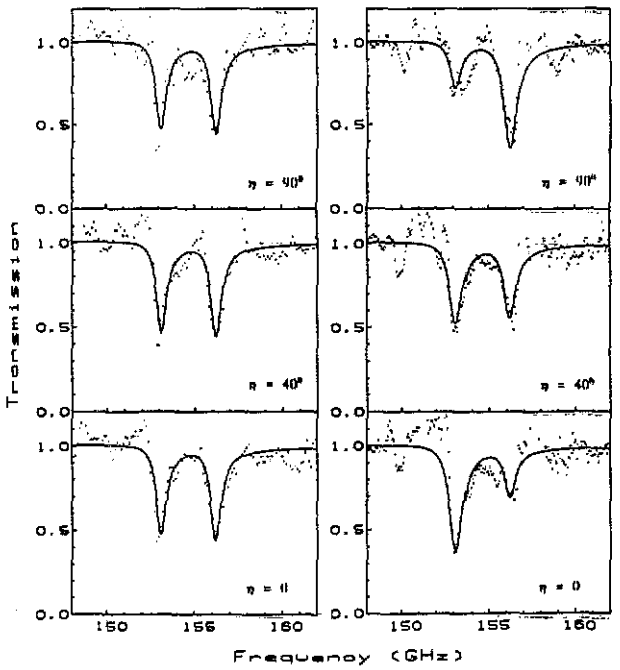

Figure 5. Zero-field splitting of the antiferromagnetic resonance in Rb_2MnCl_4, as observed in the transmission spectra for $\eta = 0°$, $\eta = 40°$ and $\eta = 90°$ (on the left-hand side) after cooling the sample in zero magnetic field from room temperature down to 4 K and (on the right-hand side) after performing a spin-flop cycle at low temperature. For details of the spin-flop cycle see the text.

an external magnetic field. These revealed that the splitting of the zero-field AFMR is observable in a number of samples and that the frequency difference of the two absorption lines does not depend on the sample. However, the (unequal) intensities of the lines turned out to be sample-dependent. Even for one sample, this ratio can be changed drastically when the sample is subjected at low temperatures to a magnetic field larger than the spin-flop critical field ($H_C = 5.55$ T for Rb_2MnCl_4 [6]) for some time and then the magnetic field is reduced to zero again. When the sample is cooled down to 4.2 K from room temperature in zero magnetic field, the intensity ratio for the two lines was always close to one (see figure 5 (left-hand side)). The transmission curves obtained with the spectrometer in Würzburg are shown in figure 5 and the following figures. They represent the transmission of the sample normalized in the way described by Geick *et al* [13]. After cycling through the spin-flop at low temperatures as described above, the intensity ratio of the two resonance lines becomes rather unequal (see figure 5 (right-hand side)). For these lines with unequal intensities (after spin-flop), the data in figure 5 show convincingly that the line intensity depends also, quite unexpectedly, on the direction of polarization of the incident light. In figure 5, the angle η is the angle between the crystallographic a-axis and the direction of polarization of the magnetic field of the electromagnetic wave in the plane perpendicular to the c axis. For $\eta = 0°$, the mode with the lower frequency at 153 GHz is more intense than the mode with the higher frequency at 156 GHz. For $\eta = 40°$, the intensities of the two modes appear to be almost equal; and for $\eta = 90°$, the intensities of the two modes are exchanged as compared with the

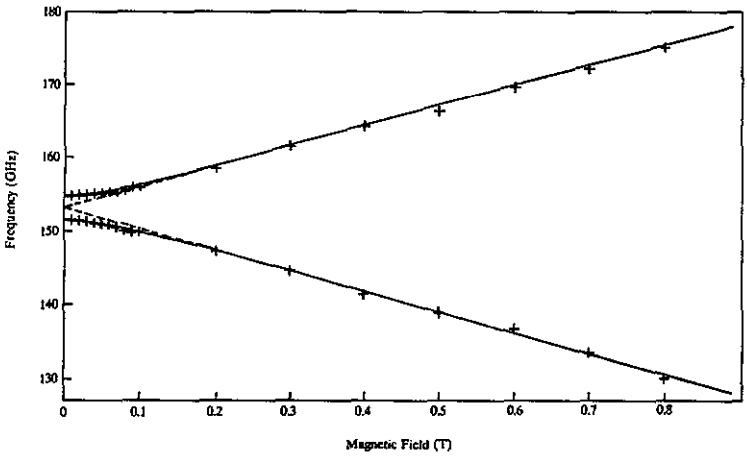

Figure 6. Frequencies of the magnon modes of Rb_2MnCl_4 as a function of magnetic field in the configuration $H_0 \| c$.

situation for $\eta = 0°$. For these magnetic resonance experiments, the thickness of the samples was about 1 mm. The full curves in figure 5 are the result of model calculations which will be presented in the next section. The experimental data in figure 5 are, furthermore, an example of the fact that magnetic resonance spectra obtained with backward-wave oscillators are generally rather noisy because of the fluctuation noise in these sources [13].

We have performed magnetic resonance experiments in the configuration $H_0 \| c$ by sweeping the frequency for a variety of magnetic fields between 0 and 1 T. The results (see figure 6) show that the upper of the two zero-field AFMR modes passes into the upper, linearly rising Zeeman branch, and the lower mode into the falling branch. The curved nonlinear part of these two branches due to the splitting at zero field is restricted to a rather small range of magnetic fields between 0 and 0.25 T. From the sample transmission curves (see figure 7), it is obvious that the transmission minima of the magnetic resonance lines increase with increasing magnetic field and are well above 50% for $H_0 \geq 0.25$ T. In other words, the transmission minima are anomalously low only in the range near $H_0 \approx 0$, and, for $H_0 \geq 0.25$ T, they have values above 50% as expected for circularly polarized modes. The curves in figures 6 and 7 are again the result of model calculations which fit the experimental points well. The details of these model calculations will be discussed in the next section. The experimental results in figures 6 and 7 clearly indicate that only measurements with backward-wave oscillators at small magnetic fields for $H_0 \| c$ can reveal the splitting of the zero-field AFMR and that these effects are not observable for conventional magnetic resonance by sweeping the field at fixed frequency.

4. Model considerations

In this section, model considerations and spin-wave calculations will be used to proceed towards an insight into, and an understanding of, the phenomena found experimentally and presented in the last section. Several models and possibilities have been considered

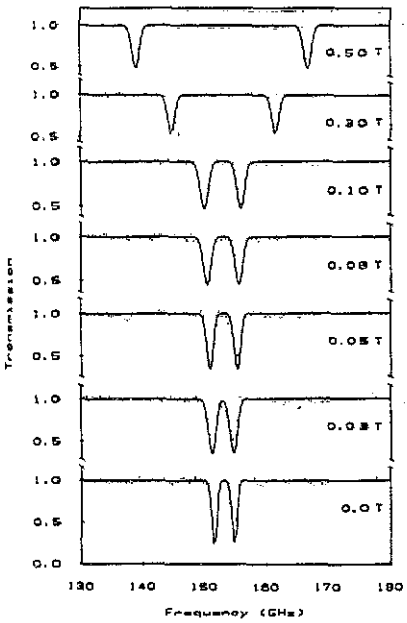

Figure 7. Antiferromagnetic resonance in Rb_2MnCl_4 for $H_0 \| c$; transmision versus frequency for various magnetic fields; ·, experimental data; ——, data calculated as described in the text.

for explaining the unusual and unexpected experimental data. Most of these ideas had to be discarded because their consequences were not in accordance with all the experimental facts and observations. Only the assumption of an orthorhombic distortion in the antiferromagnetic phase led to a satisfactory agreement between model and experiment. Most probably, this orthorhombic distortion in Rb_2MnCl_4 has the same origin as the trigonal or rhombohedral distortion observed for the antiferromagnetic state of the transition metal oxides MnO, NiO etc. [16]. In these oxides, the antiferromagnetic ordering reduces the symmetry from cubic to trigonal, and the ferromagnetic sheets within the antiferromagnetic order are planes perpendicular to the crystallographic (111) or an equivalent direction. These ferromagnetic sheets with opposite magnetization will attract each other (see figure 1 for Rb_2MnCl_4) and cause an elastic deformation along the line perpendicular to the sheets (magnetostriction, magnetoelastic effects). This deformation will only exist for non-zero sublattice magnetization below the Néel temperature and is absent in the paramagnetic state.

For comparison with the experimental results, we have performed model calculations for the magnons at wavevector $q = 0$ in Rb_2MnCl_4, including a term for the orthorhombic distortion below T_N. Our considerations are valid only for low temperatures, since we assume $\chi_\parallel \approx 0$. Our calculations start from the following energy density of the system:

$$U = (H_E/M_0)\boldsymbol{M}_a\boldsymbol{M}_b - (H_A/2M_0)[(M_a^z)^2 + (M_b^z)^2] + (\hat{H}_A/2M_0^3)[(M_a^x M_a^y)^2 + (M_b^x M_b^y)^2] - \boldsymbol{H}(\boldsymbol{M}_a + \boldsymbol{M}_b) \pm (\tilde{H}_A/2M_0)[(M_a^x)^2 - (M_a^y)^2 + (M_b^x)^2 - (M_b^y)^2]. \quad (2)$$

In equation (2), the first term describes the intra-layer exchange interaction, the second, the out-of-plane anisotropy (uniaxial symmetry), the third, the in-plane anisotropy of tetragonal symmetry, the fourth term is the Zeeman term and the last term is the in-plane anisotropy of orthorhombic symmetry representing the distortion of the crystal.

Table 1. Values of magnetic parameters for Rb_2MnCl_4.

Exchange field	$H_E = 87.09$ T†
Out-of-plane anisotropy field	$H_A = 175.5$ mT‡
In-plane anisotropy field (tetragonal symmetry)	$\hat{H}_A = 15.0$ mT‡
In-plane anisotropy field (orthorhombic symmetry)	$\tilde{H}_A = 3.6$ mT‡
Sublattice magnetization	$M_0 = 143.5$ mT§ $= 1.138 \times 10^5$ A m^{-1}

† From inelastic neutron scattering [7].
‡ From the present magnetic resonance studies.
§ Calculated from crystallographic data.

The upper sign (+) refers to one of the domains and the lower sign (−) to the other domain. $\boldsymbol{M}_a$ and $\boldsymbol{M}_b$ denote the two sublattice magnetizations with dynamic and static components, the latter with modulus M_0; H_E, $\tilde{H}_A$, $\hat{H}_A$ and H_A are the exchange field and the various anisotropy fields, respectively. The energy density U in equation (2) is restricted to those terms where the values of the parameters can be determined uniquely from our experimental data, except for the exchange field H_E which is determined from the magnon dispersion curves [7]. In particular, H_A and $\hat{H}_A$ are evaluated from the zero-field AFMR and its splitting, while $\tilde{H}_A$ is determined from the frequency of the field-independent mode in the spin-flop regime [13]. The values of the parameters are compiled in table 1†. Finally, $\boldsymbol{H}$ in equation (2) is the external magnetic field, containing the static field H_0 and the magnetic field h of the incident electromagnetic wave.

The calculation of the magnon frequencies from equation (2) proceeds along the usual lines as described by F Keffer [17] and R Geick and K Strobel [10]. For $H_0 \parallel c$ in the antiferromagnetic regime ($H_0 < H_{C\text{spin-flop}}$), we obtain the frequencies of the two magnon modes as follows (γ is the gyromagnetic ratio)

$$\nu_{1,2}^2 = \gamma^2[2H_E H_A + H_0^2 \pm \sqrt{(2H_E\tilde{H}_A)^2 + 4H_0^2(2H_E H_A)}]. \tag{3}$$

Equation (3) yields for $H_0 = 0$ the splitting of the zero-field AFMR:

$$\nu_{1,2}^2 = \gamma^2[2H_E(H_A \pm \hat{H}_A)] \tag{3a}$$

and for sufficiently large fields H_0, i.e. if $4H_0^2 \gg (2H_E\tilde{H}_A)^2/(2H_E H_A)$, the expression for the magnon frequencies of a uniaxial antiferromagnetic is obtained as an approximation to equation (3):

$$\nu_{1,2} = \gamma[\sqrt{2H_E H_A} \pm H_0]. \tag{3b}$$

The eigenvectors of the two modes in equation (3*a*) are such that for one of the domains the mode with frequency ν_1 can be excited with polarization $h \parallel a$ and the mode with frequency ν_2 with polarization $h \parallel b$. For the other domain, the polarizations have to be exchanged for the excitation of the two modes. Within our model, we have further calculated the dynamic magnetic susceptibility, and in conjunction with Maxwell's equations, the optical constants and finally the transmission of the sample (thickness

† From equation (1), the sublattice magnetizations are expected to be presented in amperes per metre. For our further model calculations, however, it is more appropriate to express the value of M_0 in teslas. For these reasons, M_0 is given in both units in table 1.

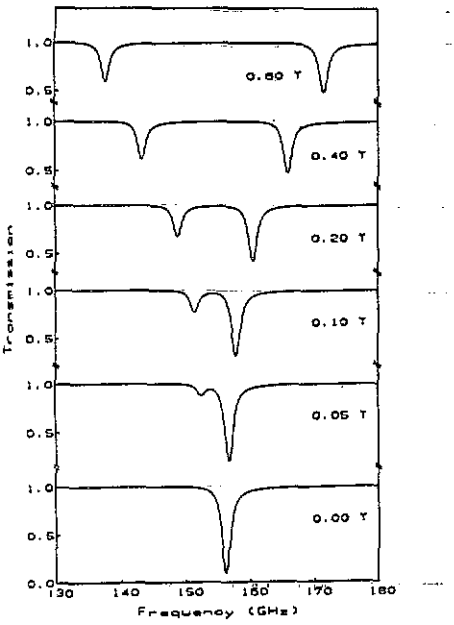

Figure 8. Antiferromagnetic resonance in Rb_2MnCl_4 for $H_0 \| c$; calculated transmission curves versus frequency for a single-domain sample (domain 1, $c = 1$). The polarization angle is $\eta = 0°$.

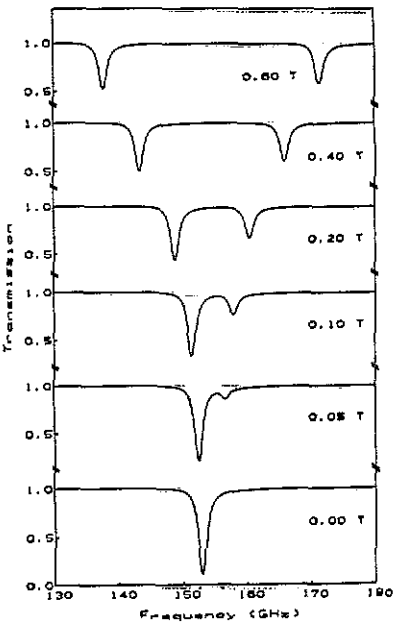

Figure 9. Antiferromagnetic resonance in Rb_2MnCl_4 for $H_0 \| c$; calculated transmission curves versus frequency for a single-domain sample (domain 1, $c = 1$). The polarization angle is $\eta = 90°$.

$d = 0.90$ mm). Here it is assumed that the sample consists of one of the domains (i.e. a single-domain sample). In figures 8 and 9, we present the results of this calculation for polarization angles $\eta = 0°$ and $\eta = 90°$, respectively. As already expected from the discussion of the eigenvectors of the modes, only one of the two zero-field AFMR modes appears in the spectrum for $\eta = 0°$, and the other one in the spectrum for $\eta = 90°$. This is certainly not in agreement with our experimental data (cf. figures 3, 5–7). Most probably the reason for this discrepancy is that we assume the sample to be single-domain. We have therefore extended the model towards multi-domain samples by means of a virtual-crystal approximation. In detail, we have calculated the dynamic magnetic permeabilities $\mu_{\text{domain 1}}$ and $\mu_{\text{domain 2}}$ for domains 1 and 2 along the lines of our spin-wave model. In order to model a multi-domain sample, we have then introduced the following effective permeability:

$$\mu_{\text{eff}} = c\mu_{\text{domain 1}} + (1 - c)\mu_{\text{domain 2}} \tag{4}$$

where c measures the portion of domain 1 in the multi-domain sample. This model requires the size of the domains to be rather small, smaller than the wavelength, so that we can treat the sample like, for example, a mixed crystal. Using μ_{eff} for the calculation of the transmission of the sample with a value $c = 0.4$, the curves in figure 7 are obtained, which agree quite well with the experimental data. From neutron diffraction experiments, it is known that Rb_2MnCl_4 crystals are multi-domain and not single-domain below the Néel temperature [18] and that a spin-flop cycle as decribed above increases the portion of one domain to the disadvantage of the other. And it is this growth of the portion of one domain in comparison to the other which explains the data presented in

figure 5. Within our model, these effects are described by a change of the value of c. Actually, the transmission curves in figure 5 have been calculated with $c = 0.5$ (before the spin-flop cycle, figure 5 (left-hand side)) and with $c = 0.25$ (after the spin-flop cycle, figure 5 (right-hand side)). In this way, we achieve good agreement between calculated and experimental data (cf. figure 5). Further, the eigenvectors of the modes, as discussed above, account well for the polarization dependence of the transmission data in figure 5, especially on the right-hand side, where one of the domains is dominant after the spin-flop cycle.

A further satisfactory aspect of our model is that it accounts well for the oscillator strengths $\Delta\mu_k$ of the two modes as defined in equation (1). Within the framework of the model (cf. equations (2) and (4)), we obtain for the oscillator strengths [10] of the modes $\Delta\mu_1 = cH_E/M_0$ and $\Delta\mu_2 = (1 - c)H_E/M_0$. With $c = 0.45$ and the values for H_E and M_0 in table 1, the model yields $\Delta\mu_1 = 0.74 \times 10^{-3}$ and $\Delta\mu_2 = 0.91 \times 10^{-3}$, in good agreement with values resulting from the simple oscillator fit (see equation (1)). Thus, the model based upon equation (2) in conjunction with equation (4) enables us to describe and also to understand all the experimental observations presented in section 3. In the next section, we will present further experimental results obtained in the configuration $H_0 \perp c$. Our model will also be applied to these data in order to show that it works well in this case, too.

5. Results for $H_0 \perp c$

The unexpected mode splitting and the β dependence of the magnetic resonance data in the configuration $H_0 \perp c$ have also prompted new experiments with the backward-wave oscillators. Only a few measurements have been made by sweeping the magnetic field for investigating the field-dependent mode at higher fields. Most of the measurements were performed by sweeping the frequency at fixed field. By this method the field-independent mode could also be observed. For $H_0 \perp c$, the spin-wave calculation yields for the frequencies of the two magnon modes

$$\nu_{1,2}^2 = \gamma^2[2H_E H_A + \tfrac{1}{2}H_0^2 \pm \sqrt{(\tfrac{1}{2}H_0^2 \pm 2H_E\tilde{H}_A \cos^2\beta)^2 + (2H_E\tilde{H}_A \sin 2\beta)^2}] \qquad (5)$$

where the notation is the same as in equations (2) and (3). The upper sign in front of the square-root refers to the field-dependent mode with frequency ν_1, the lower sign to the field-independent mode with ν_2. The upper sign in front of the term $2H_E\tilde{H}_A$ refers to one of the domains and the lower sign to the other domain. The results in equation (5) demonstrate that the orthorhombic distortion ($\tilde{H}_A$) introduces a β dependence of the frequencies which is absent without it. The eigenvectors resulting from the spin-wave calculation are such that the field-dependent mode can be observed with polarization $h \perp H_0$ and the field-independent mode with $h \parallel H_0$.

Some experimental data are presented in figure 10. Apart from the splitting, the data in figure 10 show the frequencies of the two modes as a function of H_0, namely the field-dependent mode with increasing frequency and the field-independent mode with nearly constant frequency. In figure 10, we have selected experimental data for $\beta = 0°$ (H_0 parallel to the a axis), for $\beta = 24°$ and for $\beta = 45°$ (H_0 parallel to the face diagonal between a and b axis). These three cases have been selected because they show the three different types of splitting. Because of the 2β dependence in equation (5), we obtain for $\beta = 66°$ and for $\beta = 90°$ the same type of splitting as for $\beta = 24°$ and $\beta = 0$, respectively. It is further interesting to note (cf. figure 10) that both modes have been observed with

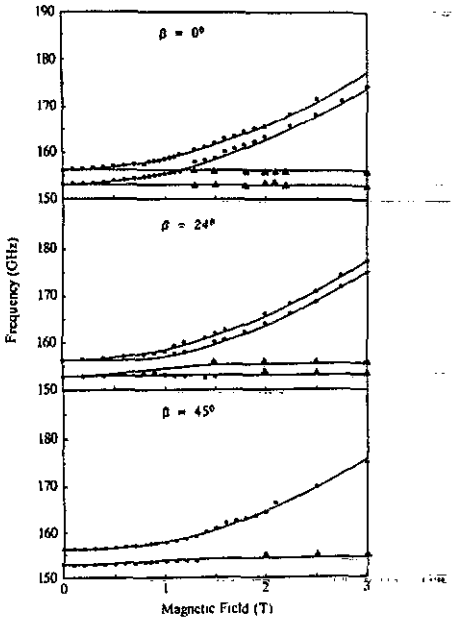

Figure 10. Antiferromagnetic resonance in Rb_2MnCl_4 for $H_0 \perp c$; magnon frequencies versus magnetic field H_0 for various orientations β of H_0 with respect to the a axis; ●, experimental points for $h \perp H_0$; ▲, experimental points for $h \parallel H_0$; ——, calculated data.

the same linear polarization for small magnetic fields ($0 \leq H_0 \leq 1$ T). This indicates that there is a rotation of the eigenvectors of the modes from those at $H_0 = 0$ to those expected for $H_0 \perp c$ which extends over this range of magnetic field.

The resonance curves in figure 10 calculated with our model again show good agreement with the experimental data. Also, we learn from the model calculations that the splitting is due to the orthorhombic distortion on the one hand and to the influence of the two domains on the other hand. This is also demonstrated by another example, shown in figure 11. Here, we have selected the experimental data for one frequency ($\nu = 161$ GHz) for a wider range of β ($0 \leq \beta \leq 400°$). Although not all data have been measured by sweeping the magnetic field, they are presented here traditionally as magnetic field at resonance versus angle β. The β dependence of the resonance field observed here for Rb_2MnCl_4 is the same as that shown in figure 2 for $(CH_3NH_3)_2MnCl_4$. When we compare the experimental data with those calculated by means of our model, it becomes clear that no splitting of the mode occurs. What appears to be a splitting is simply the superposition of the data for domain 1 and of those for domain 2. Figure 11 shows that the β-dependent curves for domain 1 and domain 2 are shifted by 90° with respect to each other, since going from one domain to the other means a change of sign in front of $2H_E\tilde{H}_A \cos 2\beta$ which is equivalent to a shift of 90° in β. All this results from the fact that the a- and b-axes exchange their roles in the two domains.

As already mentioned, we have also tried to describe and analyse our data by somewhat different model approaches. Instead of two sublattices, we have introduced four magnetic sublattices in the magnetic structure of Rb_2MnCl_4. Our analysis has shown that such a model yields four resonance modes. Two of them are acoustic-like AFMR modes as discussed above and the other two are exchange or optic-like modes. The difference between the frequency of an acoustic-like mode and that of the corresponding optic-like one turns out to be rather small in this case since it is due to the small interlayer exchange interaction. It was hoped to explain the unexpected splittings in the spectra

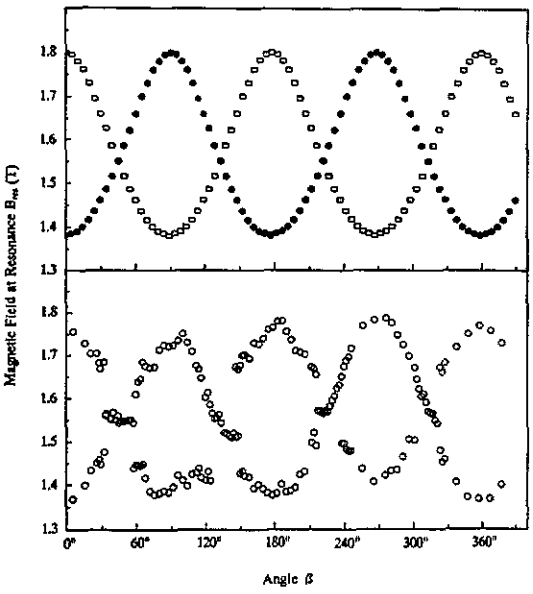

Figure 11. Magnetic field at resonance for $\nu = 161$ GHz for the configuration $H_0 \perp c$ in dependence on the angle β between H_0 and the a axis. Upper part: results of model calculation; ●, domain 1; □, domain 2; and lower part: experimental data, ○.

by means of this small difference. But a careful analysis shows that the four modes are not all equally optical active. The acoustic-like modes can be observed as usual AFMR modes by magnetic resonance. In a perfect crystal, the optic-like modes belong to magnons at the Z-point at the edge of the Brillouin zone and can be observed optically at $\boldsymbol{q} = \boldsymbol{0}$ only when there is a disorder in the layer packing, i.e. no perfect translational symmetry along the c direction. Since such effects have not been observed and since this model cannot explain the sample-dependent unequal intensities of pairs of modes, we have abandoned the four-sublattice model in favour of the two-sublattice model which allows us to describe satisfactorily all experimental data.

In our model, we have described the orthorhombic distortion below the Néel temperature by the additional in-plane anisotropy of orthorhombic symmetry. But there may be other types of anisotropic interactions of orthorhombic symmetry which could be included in our model considerations. Such an anisotropic interaction is, for example, the Dzyaloshinskii–Moriya interaction $\boldsymbol{D}(\boldsymbol{M}_a \times \boldsymbol{M}_b)$. In Rb_2MnCl_4, this interaction is allowed by symmetry only for $D_z \neq 0$ below T_N and not for $D_x \neq 0$ as it is the case for La_2CuO_4 with a similar orthohombic structure [19]. For $D_x \neq 0$, the antisymmetric exchange interaction effectively induces a torque on the sublattice magnetizations but not for $D_z \neq 0$ in Rb_2MnCl_4. Moreover, we did not want to include further terms in equation (2) with additional parameters which cannot be uniquely determined from the experimental data, as is now the case.

6. Conclusions

Our magnetic resonance studies of Rb_2MnCl_4 have revealed that, in contrast to the knowledge available so far:

(i) there is a splitting of the zero-field AFMR. For $H_0 > 0.25$ T in the configuration $H_0 \| c$, these split modes pass into the usual Zeeman branches without an indication of a splitting of these branches;

(ii) there seems to be a splitting of the magnetic resonance data for $H_0 \perp c$. In this configuration, the magnetic resonance data show a dependence on the angle β between H_0 and the a-axis;

(iii) there are unequal intensities of the two modes of the zero-field AFMR. The ratio of these intensities depends on the sample and on the pretreatment of the sample.

Our analysis of the results by means of a model calculation led us to the conclusion that the observed phenomena are due to an orthorhombic distortion of Rb_2MnCl_4 below its Néel temperature. They can be explained on the basis that there are two antiferromagnetic domains and that all samples are multi-domain and not single-domain. This orthorhombic distortion is probably small. It has not yet been directly verified by x-ray or neutron diffraction experiments. Our model calculations are based on the usual energy density for a uniaxial antiferromagnet with an additional anisotropy term modelling the orthorhombic distortion. A virtual-crystal approximation takes account of the multi-domain character of our samples. In this way, the calculated model data agree well with the experimental values.

There are some indications that the phenomena observed in this investigation for Rb_2MnCl_4 are not restricted to this material. In figure 2, it was shown that the β dependence of the magnetic resonance for $H_0 \perp c$ has also been found for $(CH_3NH_3)_2MnCl_4$. In brief preliminary experiments, we have observed the splitting of the zero-field AFMR in K_2MnF_4 as well. It seems therefore that the effects discussed here for Rb_2MnCl_4 may be a property of the whole class of quasi-two-dimensional antiferromagnets with the K_2NiF_4 structure.

Finally, we can measure the portions of the two antiferromagnetic domains in these materials by comparing the intensities of the two zero-field AFMR modes. This information is usually obtained by neutron diffraction from the intensities of the $(\frac{1}{2}, \frac{1}{2}, 0)$ and the $(\frac{1}{2}, -\frac{1}{2}, 0)$ antiferromagnetic super-reflections. This means such a neutron scattering experiment can in principle be replaced by a magnetic resonance measurement.

Acknowledgments

This work has been funded by the Bundesministerium für Forschung und Technologie under contact 03-Ge-2-Wue-3. Some of us (HG, TP, MR, KS and RG) gratefully acknowledge financial support by the Deutsche Forschungsgemeinschaft.

References

[1] de Jongh L J and Miedema A R 1974 *Adv. Phys.* **23** 1
[2] Epstein E, Gurewitz E, Makowsky J and Shaked H 1970 *Phys. Rev.* B **2** 3703
[3] Fedoseeva N V, Spevakova I P, Bazhan A N and Beznosikov B V 1978 *Sov. Phys. Solid State* **20** 1600
[4] Deonarine S and Joshua S J 1976 *Phys. Status Solidi* b **74** 659
[5] de Groot H J M and de Jongh L J 1986 *Physica* B **141** 1
[6] Rauh H, Erkelens W A C, Regnault L P, Rossat-Mignod J, Kullmann W and Geick R 1986 *J. Phys. C: Solid State Phys.* **19** 4503
[7] Schröder B, Wagner V, Lehner N, Kesharwani K M and Geick R 1980 *Phys. Status Solidi* b **97** 501
[8] Strobel K and Geick R 1981 *Physica* B **108** 951

[9] Grieb T, Strobel K and Geick R 1984 *Solid State Commun.* **51** 923
[10] Geick R and Strobel K 1983 *Reviews on Infrared and Millimeter Waves* vol 1 ed K J Button (New York: Plenum) p 249
[11] Reusch W, Strobel K and Geick R 1981 *Digest of the Sixth Int. Conf. on Infrared and Millimeter Waves (Miami Beach 1981)* paper T-2-2
[12] Greb H and Geick R 1989 *Infrared Phys.* **29** 765
[13] Geick R, Greb H, Hock B, Jaitner H, Maier D, Pabst T, Treutmann W and Hosoya S 1991 *Infrared Phys.* **32** 91
[14] Balbashov A M, Volkov A A, Lebedev S P, Mukhin A A and Prokhorov A S 1985 *Sov. Phys.–JETP* **61** 753
[15] Volkov A A, Goncharov Yu G, Kozlov G V, Lebedev S P and Prokhorov A M 1985 *Infrared Phys.* **25** 369
[16] Roth W L 1958 *Phys. Rev.* **110** 1333
[17] Keffer F 1966 *Encyclopedia of Physics* vol XVIII/2, ed S Flügge (Heidelberg: Springer) p 1
[18] Kullmann W, Hirte J, Weitzel H, Lehner N and Geick R 1982 Spin-flop phase transition and magnetic phase diagram of Rb_2MnCl_4 *Institut Laue–Langevin Experimental Report*
[19] Bar'yakhtar V G, Loktev V M and Yablonskii D A 1988 *Physica* C **156** 667